Journal of Catalysis 257 (2008) 23–31

Contents lists available at ScienceDirect

Journal of Catalysis

www.elsevier.com/locate/jcat

SBA-15-based polyamidoamine dendrimer tethered Wilkinson's rhodium complex for hydroformylation of styrene

P. Li, S. Kawi *

Department of Chemical & Biomolecular Engineering, National University of Singapore, 10 Kent Ridge Crescent, Singapore 119260, Republic of Singapore

ARTICLE INFO

Article history:
Received 14 February 2008
Revised 3 April 2008
Accepted 4 April 2008
Available online 21 May 2008

Keywords:
Dendritic catalysts
Dendrimer
Hydroformylation
SBA-15
$HRh(CO)(PPh_3)_3$
Styrene

ABSTRACT

Dendritic SBA-15 supported $HRh(CO)(PPh_3)_3$ catalysts were designed for liquid-phase hydroformylation of styrene. The silanols outside SBA-15 channels were passivated so that $HRh(CO)(PPh_3)_3$ complexes could be anchored mostly inside the SBA-15 channels. After passivation, PAMAM (polyamidoamine) dendrimers up to second generation were then grown inside the SBA-15 channels. Both pore size and dendrimer generation were found to influence the performance of catalysts for styrene hydroformylation, and the second-generation PAMAM was found to be optimal for these passivated dendritic SBA-15-supported rhodium catalysts. To study the effect of tethering $HRh(CO)(PPh_3)_3$ inside and outside SBA-15 mesopore channels, we also studied SBA-15-supported catalyst analogs with no passivation of external silanols. The passivated SBA-15 supported rhodium catalysts demonstrated an increase in catalytic activity and stability when the generation of supported dendrimer was increased from zeroth to second generation.

1. Introduction

Ever since Roelen's serendipitous discovery of hydroformylation in a Fisher–Tropsch catalytic reaction in 1938, hydroformylation has developed into the most widely used homogeneously catalyzed industrial process. Over the past several decades, much effort has been directed toward the synthesis of highly active and selective catalysts for the hydroformylation reaction, using different transition metals and various ligands. Rhodium complexes are the most widely applied and studied catalysts. Rhodium-based hydroformylation catalysts can be applied in relatively milder reaction conditions [1]. Detailed studies on homogeneous $HRh(CO)(PPh_3)_3$ complex for hydroformylation reactions have been reported [2]. However, homogeneous hydroformylation reactions face the problems of separation of transition metal from the liquid phase in industry, because the separation process is not only energy-intensive and time-consuming, but also corrosive to equipment and unfriendly to the environment. Consequently, producing heterogenized hydroformylation catalysts for industry is a desirable goal. Much recent research has been aimed at synthesizing a heterogenized hydroformylation catalyst combining the advantages of the heterogeneous and homogeneous catalytic systems [3].

Many solid supports (e.g., alumina, resin) have been used as catalyst supports to anchor rhodium complexes [4,5]. Among the solid supports, the family of mesoporous materials, such as MCM-41, is particularly promising due to their highly ordered mesoporous structures and high surface areas [6,7]. Another promising family of catalyst supports is dendrimer, an ideal support for transition metal complexes. When dendrimer is terminated with amine and phosphine ligands, not only do the lone pair electrons bind and influence the guest transition metal, but also the multiple catalytic centers may cooperatively enhance activity and selectivity. Dendrimer also has been used as a catalyst support [8,9].

Reynhardt et al. investigated the combination of PAMAM dendrimer with MCM-41 for the synthesis of heterogenized hydroformylation catalysts [7] and found their MCM-41-based first-generation dendritic catalyst to be both active and selective. However, the pore size distribution of MCM-41 (which has a pore diameter of around 6 nm) was not large enough for hosting higher-generation dendrimers to provide more sites for anchoring rhodium complex species. Therefore, the MCM-41-based dendritic catalyst did not demonstrate good catalytic performance in its second-generation PAMAM-based MCM-41-supported catalyst [7].

To anchor higher-generation dendrimer on mesoporous support to improve the catalytic performance, SBA-15 (which has a uniform mesopore diameter of around 8 nm) was used to grow second-generation PAMAM dendrimers [10]. Hydrido rhodium carbonyl triphenylphospine complex ($HRh(CO)(PPh_3)_3$) was then tethered on the dendrimer supported on SBA-15. Furthermore, to study the pore effect on the catalytic performance of SBA-15-based PAMAM dendrimer-supported rhodium catalyst, passivation of silanols outside the SBA-15 mesopore channels was applied, to ensure sure that the dendrimers were anchored mainly inside the mesopores of SBA-15 [6,11,12].

* Corresponding author.
E-mail address: chekawis@nus.edu.sg (S. Kawi).

0021-9517/$ – see front matter
doi:10.1016/j.jcat.2008.04.002

2. Experimental

2.1. Chemicals

3-Aminopropyltriethoxysilane (APES), dichlorodiphenylsilane (Ph_2SiCl_2), methyl acrylate (MA), and ethylenediamine (EDA) were purchased from Aldrich. $HRh(CO)(PPh_3)_3$ (Wilkinson's complex), used as the rhodium precursor, was purchased from Strem Chemicals. Reactions involving air-sensitive compounds were performed using a Schlenk line under a positive pressure of purified nitrogen. Transfer of rhodium complexes was done inside a LABCONCO glove box purged with dried N_2. All solvents were dried and distilled before use.

2.2. Synthesis and pre-treatment of SBA-15

SBA-15 was prepared following the synthesis procedures reported previously [10]. The SBA-15 support was then pretreated under vacuum at 200 °C for 12 h to remove physically adsorbed water molecules before functionalization.

2.3. Functionalization of SBA-15

In this study, we used two methods to functionalize the internal pore surfaces of SBA-15. The first method was to directly functionalize SBA-15 with a monolayer of amine ligands, followed by grafting of PAMAM dendrimers on these amine ligands. The second method was to passivate the external silanols outside the SBA-15 channels, then functionalize the internal SBA-15 surfaces with a monolayer of amine ligands, and, finally, graft the PAMAM dendrimers.

2.3.1. Functionalization of SBA-15 without passivation

Functionalization of SBA-15 without passivation was carried out via traditional functionalization of the surface silanols with APES to give aminated SBA-15 (NH_2). These amine groups act as "initiator sites" that form zeroth-generation dendrimer, from which higher generations of dendrimers can be grown. Typically, 5.0 g of SBA-15, 150 ml of toluene, and 7.5 ml of APES were charged into a 250-ml three-necked flask. The mixture was then refluxed for 48 h under stirring with a magnetic stirrer. After functionalization, the aminated SBA-15 was filtered out and dried at 120 °C under vacuum. The resulting functionalized SBA-15 solid was designated S0 (SBA-15 with zeroth-generation dendrimer).

2.3.2. Functionalization of SBA-15 with passivation

Functionalization of SBA-15 with passivation was carried out by passivating the silanols outside the mesopores of SBA-15 before functionalization, with the remaining steps of growing dendrimers the same as those used in the functionalization of SBA-15 without passivation. Typically, 2 g of SBA-15 was dehydrated under vacuum at 200 °C for 12 h and then slurried in 60 ml of THF. Then 0.06 ml of Ph_2SiCl_2 was added to the slurry, and the suspension was stirred for another 1 h. The reaction mixture was cooled to 195 K, after which 1.0 ml of APES was added to the reaction mixture. The slurry was stirred for 3 h at 195 K, warmed slowly to ambient temperature, and then held at 50 °C for another 20 h. The reaction mixture was then filtered, and the solid was washed with copious amounts of THF (100 ml) and dried under vacuum. The resulting solid was designated PS0 (passivated SBA-15 with zeroth-generation dendrimer).

2.4. Grafting of dendrimers on aminated SBA-15

Grafting reaction and propagation of PAMAM dendrimer on the functionalized SBA-15 (S0 or PS0) were achieved by two processes [13]. Michael addition, the reaction step in grafting the first half-generation of dendrimer on SBA-15, was carried out as follows. First, 150 ml of ethanol and 2.5 ml of MA were added into a 250-ml three-necked flask containing 5 g of S0. The mixture was refluxed for 24 h under stirring with a magnetic stirrer. After the Michael reaction, the solid was filtered and washed with ethanol. The resulting solid was designated S0.5 (SBA-15 grafted with half-generation dendrimer).

Amidation of terminal ester groups, the first step in grafting the second half-generation of dendrimer on SBA-15, was carried out as follows. First, 150 ml of ethanol and 10 ml of EDA were added into the 250-ml three-necked flask containing 5 g of S0.5. The mixture was stirred with a magnetic stirrer and refluxed for 24 h. The solid collected from filtration was washed with ethanol. The resulting solid was designated S1 (SBA-15 grafted with first-generation dendrimer).

Alternate Michael addition and amidation reaction steps were then performed on S1 to propagate the dendrimer to the second generation to produce S2 (SBA-15 grafted with second-generation PAMAM dendrimer). However, the grafting of higher than second generation of dendrimer on SBA-15 was not attempted in this study, because the mesopore of SBA-15 (with a diameter of ca. 8 nm) has been found to be quite congested with grafted dendrimer [13,14].

Similarly, alternate Michael addition and amidation reaction were conducted first on PS0 to produce PS1 (passivated SBA-15 grafted with first-generation dendrimer) and then on PS1 to produce PS2 (passivated SBA-15 grafted with second-generation dendrimer).

2.5. Tethering of Rh precursor on dendritic SBA-15 support

Dendritic SBA-15 supports (S*n* or PS*n*, where *n* represents the number of generation of grafted dendrimers) were reacted with $HRh(CO)(PPh_3)_3$ by coordination of the surface ligand donors to the rhodium precursor to produce rhodium complex catalyst tethered on dendrimer grafted on SBA-15. The tethering of Rh precursor onto the dendritic SBA-15 support was carried out as described previously [15]. In brief, after 90 mg of $HRh(CO)(PPh_3)_3$ was dissolved in 60 ml of toluene, 0.5 g of dendritic SBA-15 support (PS*n* or S*n*) was added to the solution, and the resulting mixture was stirred and refluxed overnight at 70 °C under nitrogen protection (Scheme 1). The catalysts were designed to contain 2 wt% of rhodium (i.e., 0.194 mmol Rh/g of catalyst support). The preparation of tethered rhodium complex catalysts was carried out under nitrogen atmosphere to avoid exposing the catalyst to air or moisture, which could affect the activity of the supported rhodium catalyst. After cooling to room temperature, the mixture was filtered, and the separated solid was washed with toluene (4×20 ml), then dried under vacuum at room temperature.

The synthesized catalyst was designated HS*n* or HPS*n*, where H represents the $HRh(CO)(PPh_3)_3$ precursor, S represents SBA-15, P represents passivation, and *n* is the ordinal number of the generation of the grafted dendrimers. Note that all PS*n* ($n = 0, 1, 2$) and S*n* ($n = 0, 1, 2$) samples were dehydrated at 120 °C under vacuum for 12 h before being used to tether $HRh(CO)(PPh_3)_3$. The freshly made light yellow catalyst was stored in a LABCONCO glove box.

2.6. Catalytic tests

The hydroformylation reactions were carried out at 20 bar of CO/H_2 (1:1) syn-gas mixture at 60 °C with styrene as the substrate and 1-hexane as the solvent. Each reaction required 3 ml of styrene and 50 ml of solvent. For each catalytic reaction, 0.15 g of heterogenized catalyst was transferred into a Parr reactor under nitrogen atmosphere, and 1-hexane was pumped into the reactor. Once the catalytic reaction system reached the temperature required for the

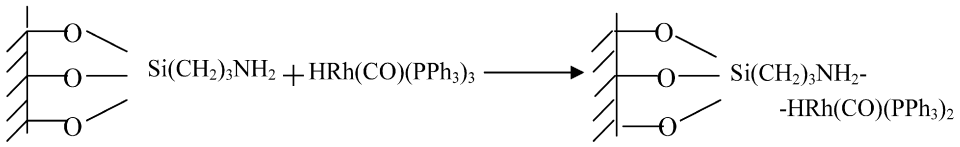

Scheme 1. Tethering of $HRh(CO)(PPh_3)_3$ on aminated SBA-15.

reaction, styrene was pumped into the Parr reactor and the entire reaction system was flushed with syn-gas before the catalytic reaction.

2.7. Characterization

The N_2 isotherms of SBA-15 samples were determined with an Autosorb-1 (Quantachrome). About 0.1 g of catalyst sample was first outgassed at 200 °C for about 8 h. Nitrogen at 77.4 K was used as the adsorbate. The specific surface areas and pore size distributions of supports were calculated according to the linear portion of the BET plot and the BJH method based on the adsorption–desorption isotherm.

X-ray photoelectron spectroscopy (XPS) was used to determine the chemical state of Rh of the fresh and used catalysts. A Shimadzu Kratos AXIS XPS spectrometer (Shimadzu, Japan), with a monochromatic Al $K\alpha$ X-ray source (1486.6 eV, 225 W) and a constant transmission pass energy of 80 eV, was used.

The infrared spectra characterizing the HPS2, UHPS2, and $HRh(CO)(PPh_3)_3$ were measured with Shimadzu FTIR-8400 spectrometer (Shimadzu, Japan). The HPS2 and UHPS2 were pressed into self-supported disks of ~15 mg. The $HRh(CO)(PPh_3)_3$ was mixed with nujol and put between KBr windows.

A Philips FEG CM300 high-resolution transmission electron microscope with an electron kinetic energy of 300 kV was used to scan the catalyst supports and used catalysts. The samples were prepared by dispersing the powders in acetone in sample vials, then dipping these vials in an ultrasonic bath for ultrasonic treatment. A drop of this well-dispersed suspension was placed on a carbon-coated 300-mesh copper grid, followed by drying aliquot under ambient conditions before TEM scanning.

A gas chromatograph with a flame ionization detector (Perkin Elmer Auto System XL) was used to identify the reactant and reaction products during or after reaction. An HP 5MS nonpolar capillary column (cross-linked 5% phenyl methyl siloxane), with a length of 30 m and a diameter of 0.25 mm, was used.

The weight percentage of rhodium metal in the fresh and used catalysts was determined by a Perkin Elmer ICP (inductively coupled plasma) atomic emission machine.

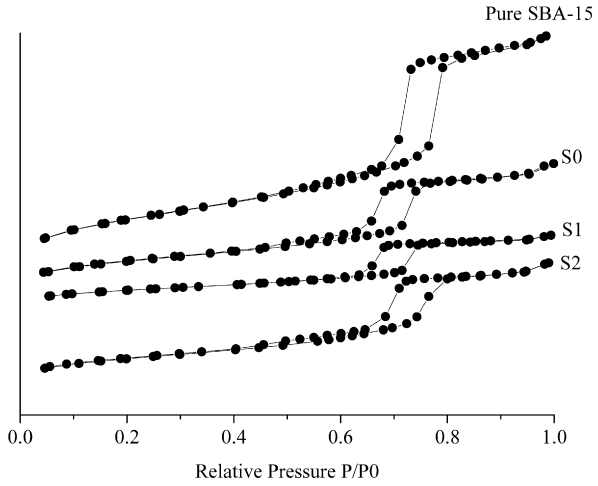

Fig. 1. N_2 adsorption–desorption isotherms of pure SBA-15, S0, S1, and S2.

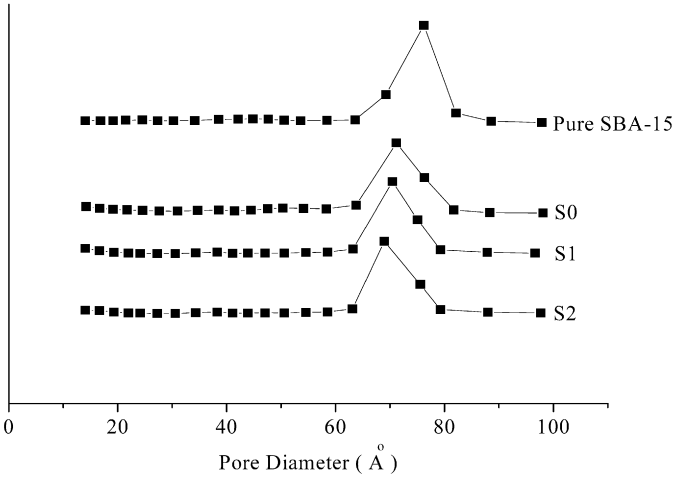

Fig. 2. Pore size distribution of pure SBA-15, S0, S1 and S2.

3. Results and discussion

3.1. Catalyst characterization

3.1.1. BET measurements

Fig. 1 shows the nitrogen-adsorption isotherms of pure SBA-15, S0, S1, and S2. The relative pressure at which capillary condensation starts to occur shifted to a lower value from pure-SBA-15 to S0. But as the dendrimer generation increased from S0 to S2, the relative pressure at which condensation began did not change much. This finding is consistent with the pore size distribution results for S0, S1, and S2 shown in Fig. 2. The pore size distributions of these nonpassivated SBA-15-based dendritic supports did not decrease much from S0 to S2. Because the hysteresis loops did not shift systematically from S0 to S2 and the pore size distributions scarcely decreased from S0 to S2, these results suggest that a considerable proportion of the dendrimer was not grown inside the mesopores [10], but instead, as the dendrimer generation increased, most of the dendrimers were grown on the external surface of the SBA-15 support [16].

Fig. 3 depicts the nitrogen-adsorption isotherms of the pure SBA-15, PS0, PS1, and PS2 catalyst supports. Obviously, as the dendrimer generation increased from PS0 to PS2, the hysteresis loops of PS0, PS1, and PS2 systematically shifted to lower relative pressures, indicating a lower relative pressure at which capillary condensation starts. This is consistent with the pore size distributions of PS0, PS1, and PS2, as shown in Fig. 4. From PS0 to PS2, the pore size distributions decreased from 69 to 59 Å. In contrast, from S0 to S2, the pore size distribution decreased only by 2 Å. These results indicate that for the passivated dendritic SBA-15 supports, the dendrimers were grown inside the mesopores, and as the dendrimer volume increased, the pore size distribution decreased accordingly [16].

All of the isotherms of the SBA-15-based dendritic supports showed a clear H1 hysteresis loop [17]. These results are consistent with our previously reported results indicating that the

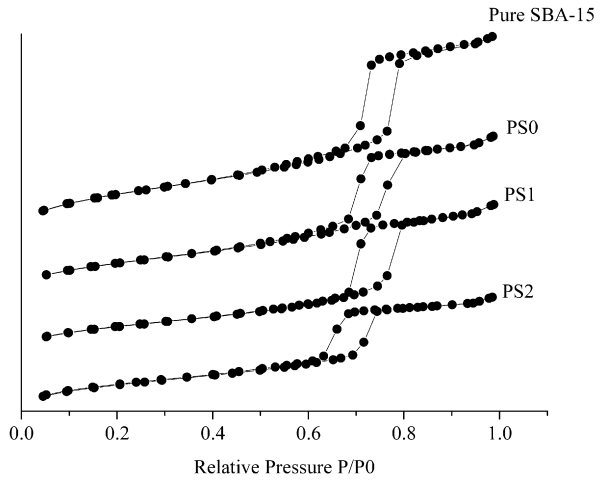

Fig. 3. N_2 adsorption–desorption isotherms of pure SBA-15, PS0, PS1 and PS2.

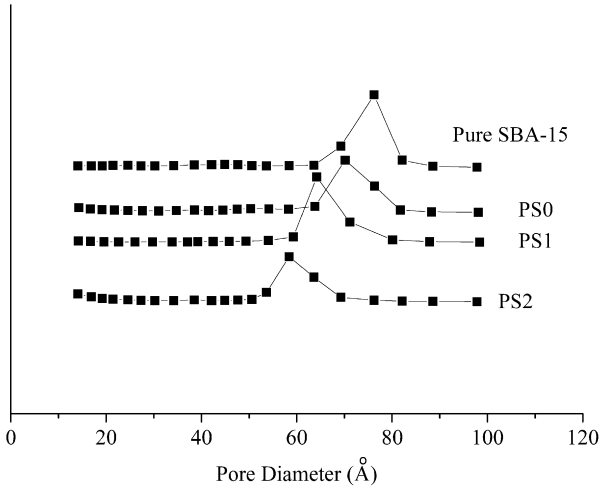

Fig. 4. Pore size distribution of pure SBA-15, PS0, PS1 and PS2.

Table 1
BET results of SBA-15 based supports

Sample	Pore size[a] (A)	Surface area (m^2/g)
Pure SBA	75	692.5
PS0	69	486.3
PS1	64	459.8
PS2	59	449.6
S0	71	387.5
S1	70	347.5
S2	69	341.4

[a] From the desorption branch of isotherm.

anchoring of dendrimer on SBA-15 up to the second generation did not destroy its highly ordered mesoporous structures [13]. As shown in Table 1, all passivated dendritic SBA-15 catalyst supports had greater surface areas than their nonpassivated SBA-15-based analogues. This may be due to the wide dispersion of PAMAM dendrimers inside the SBA-15 channels of the former, because the inner surface of SBA-15 channels has much greater area and space than the outer surface. The decreases in BET surface area and pore size distribution are consistent with those reported previously [18].

3.1.2. XPS measurements

Fig. 5 shows the XPS spectra of Rh $3d_{5/2}$ in $HRh(CO)(PPh_3)_3$ (designated "Homo" in the graph) and fresh HPS0, HPS1, and HPS2 catalysts. The binding energy (BE) value of Rh $3d_{5/2}$ in the

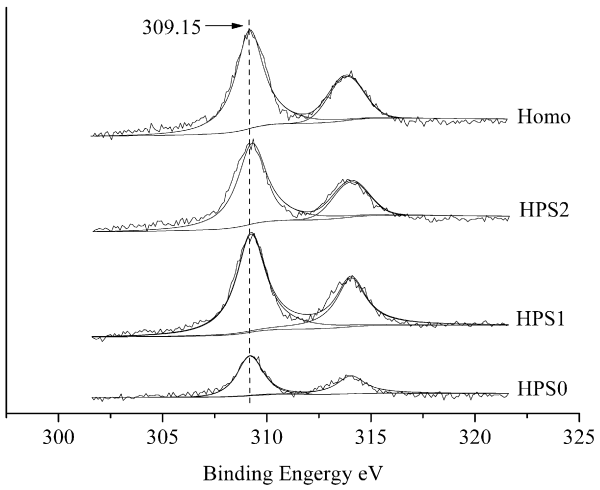

Fig. 5. XPS spectra of fresh HPSn ($n = 0, 1, 2$) catalysts ($HRh(CO)(PPh_3)_3$ as reference).

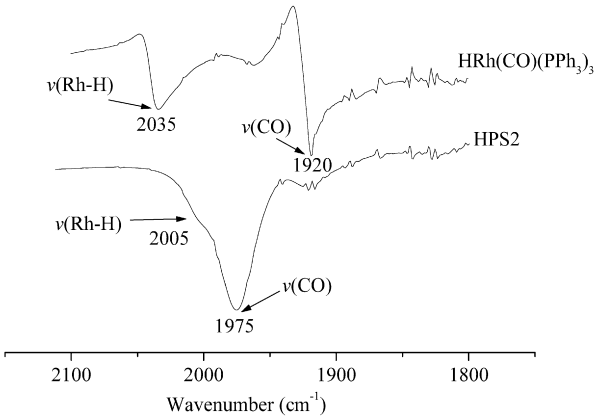

Fig. 6. FTIR spectra of $HRh(CO)(PPh_3)_3$ and fresh HPS2.

$HRh(CO)(PPh_3)_3$ precursor can be seen at 309.15 eV, in agreement with the literature [19]. The BE values of Rh $3d_{5/2}$ of all fresh HPSn catalysts deviated by <0.2 eV from that of their homogeneous precursor, $HRh(CO)(PPh_3)_3$. This demonstrates that the rhodium species tethered on these as-synthesized catalysts were present as Rh(I) species, indicating that the supported precursor retained the integrity of complex $HRh(CO)(PPh_3)_3$. The exact chemistry of the tethered moiety remains incompletely understood; a weak coordinate-covalent interaction between the terminal amine ends of PAMAM dendrimer and the Rh-center of the $HRh(CO)(PPh_3)_3$ complex has been proposed; this hypothesis is similar to that proposed by Burk et al. [20].

No significant differences in the BE values of Rh $3d_{5/2}$ were found among the fresh HPS0, HPS1, and HPS2 catalysts. This finding indicates that the interaction between the guest $HRh(CO)(PPh_3)_3$ complex and the surface ligands was similar among these catalysts, and that the pore size decrease did not reach the point at which the conformation of the tethered moiety started to deform. It also suggests that the electronic properties of the 3 heterogenized rhodium catalysts are quite similar. Therefore, the differences in catalytic performance in terms of activity and selectivity cannot be attributed to the electronic effects; rather they should be attributed to the different steric properties due to differences in dendrimer generation, pore size distribution, and surface areas of the SBA-15 dendritic-based supports.

Table 2
IR characteristics of $HRh(CO)(PPh_3)_3$ reported in literature

Authors	υ(CO) (cm^{-1})	υ(Rh–H) (cm^{-1})	Experimental conditions	Ref.
Varshavsky et al.	1926	2042	Nujol	[21]
Sharma et al.	1965	2036	KBr pellet	[23]
Scott and Rempel	1982	2020	–	[24]
Horvath et al.	1924	2008	Solvent: toluene	[25]
Trzeciak et al.	1920	2006	Solvent: dichloromethane	[26]
Bath and Vaska	1926	2004	Solvent: benzene	[27]
Evans et al.	1920	2000	Solvent: benzene, dichloromethane, cyclohexane	[2]
Mukhopadhyay et al.	1922	–[a]	–[a]	[6]

[a] –: Not reported in the references.

3.1.3. FTIR measurements

Fig. 6 shows the infrared spectra of HPS2 and $HRh(CO)(PPh_3)_3$ as the reference. In the FTIR spectrum of HPS2, the strong peak at 1975 cm^{-1} can be attributed to the terminal CO stretching [2,6]. This υ(CO) of HPS2 of ca. 1965 cm^{-1} is close to the υ(CO) of $HRh(CO)(PPh_3)_3$ supported inside the functionalized MCM-41 mesopores [6]. The υ(CO) of HPS2 exhibited a higher wavenumber than the υ(CO) of the unsupported $HRh(CO)(PPh_3)_3$ [21], indicating back-donation from the supported Rh center to CO, resulting in a strengthened C–O bond [22]. The weaker π back-donation from Rh exhibited a decreased electron density around the Rh center in HPS2, indicating that the surface amine ligands on SBA-15 may have slightly displaced the PPh_3 ligand out of the coordination sphere around the Rh center. The FTIR spectrum of HPS2 suggests that the supported $HRh(CO)(PPh_3)_3$ differed somewhat from the $HRh(CO)(PPh_3)_3$ precursor, indicating that this Rh precursor reacted with the surface functional group during the tethering process.

Table 2 lists the wavenumbers of υ(CO) and υ(Rh–H) peaks of $HRh(CO)(PPh_3)_3$ reported in the literature. The table shows that the FTIR positions of υ(CO) and υ(Rh–H) were sensitive to the environment during FTIR measurement, with υ(CO) ranging from 1920 to 1982 cm^{-1} and υ(Rh–H) ranging from 2000 to 2042 cm^{-1} [2,6,21,23–27].

A broad shoulder peak at around 2005 cm^{-1} was seen in the FTIR spectrum of HPS2, attributed to the υ(Rh–H) of the dendritic SBA-15-supported $HRh(CO)(PPh_3)_3$. The υ(Rh–H) peak observed in HPS2 was not strong; υ(Rh–H) is typically very weak and easily obscured [28].

3.1.4. TEM images

TEM is widely used for the structural elucidation of mesoporous materials and has proven very useful in this application. To study the mesoporous structures of the passivated dendritic SBA-15 catalyst supports, we characterized PS0, PS1, and PS2 by TEM (Figs. 7a–7c). All TEM images were taken perpendicular to the SBA-15 channels. The TEM results are consistent with the BET results, demonstrating a uniform pore size distribution with a hexagonal array of one-dimensional mesopore channels and a two-dimensional *p6mm* hexagonal of SBA-15, as reported by Zhao et al. [10].

3.1.5. Elemental analysis

Along with the FTIR and TGA measurements [13], elemental analysis also was used to quantify the amount of dendrimers grown on the surfaces of the catalyst supports [29]. Table 3 gives the weight contents of C, H, and N on the passivated and nonpassivated dendritic SBA-15 catalyst supports. The increased weight percentage of C, H, and N on both passivated and nonpassivated catalyst supports with increasing dendrimer generation confirms the successful grafting of dendrimer on the supports. Comparing the passivated and nonpassivated dendritic supports at the same generation shows higher C, H and N contents in PS0, PS1, and PS2 than in S0, S1 and S2, respectively. This finding indicates that dendrimers were grown more ideally and completely on the passivated SBA-15 catalyst supports. For the nonpassivated SBA-15 supports, the hindered growth of dendrimer is attributed to the crowding of

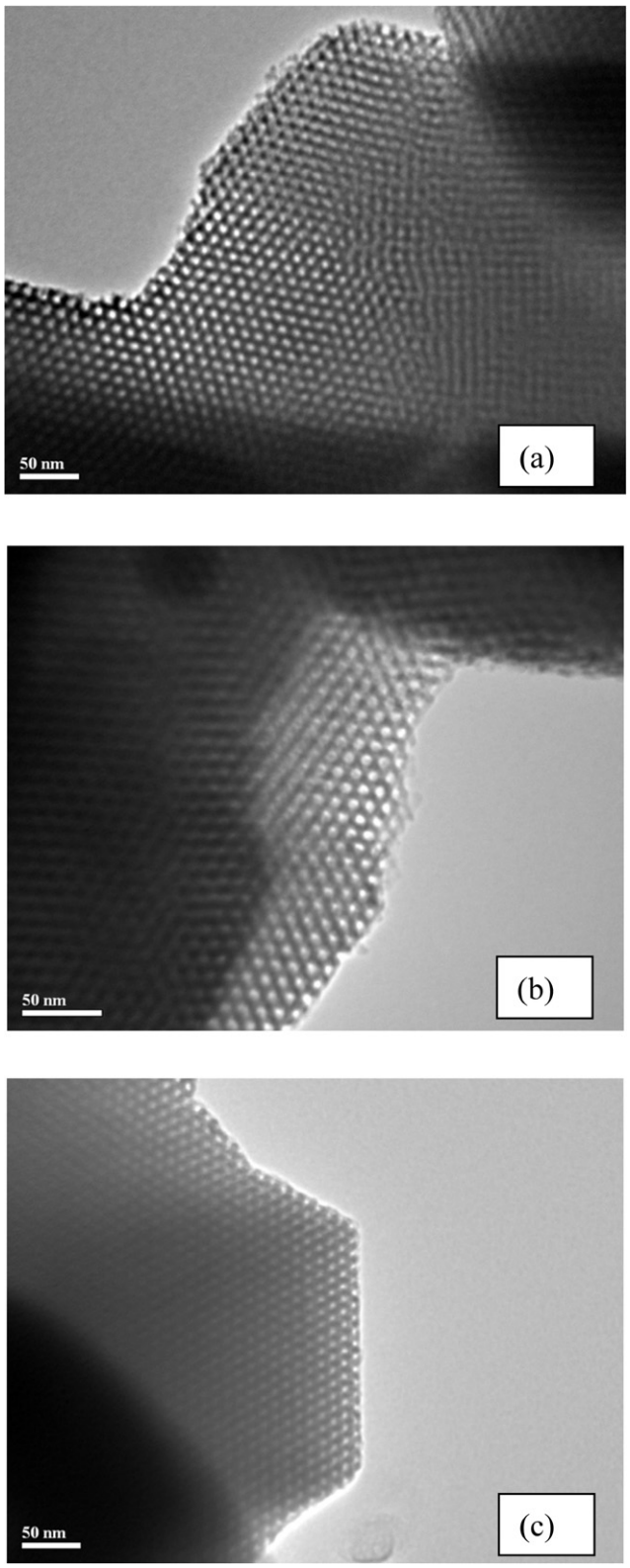

Fig. 7. TEM image of (a) PS0, (b) PS1 and (c) PS2 catalyst supports.

Table 3
C, H, N analysis of SBA-15 based supports

Sample	Carbon (%)	Hydrogen (%)	Nitrogen (%)
Pure SBA-15	0.25	1.55	0.22
S-0	8.60	1.88	2.93
S-1	13.12	2.33	3.24
S-2	13.91	2.54	4.06
PS-0	10.78	2.63	2.84
PS-1	17.33	2.92	3.65
PS-2	18.55	3.22	4.36

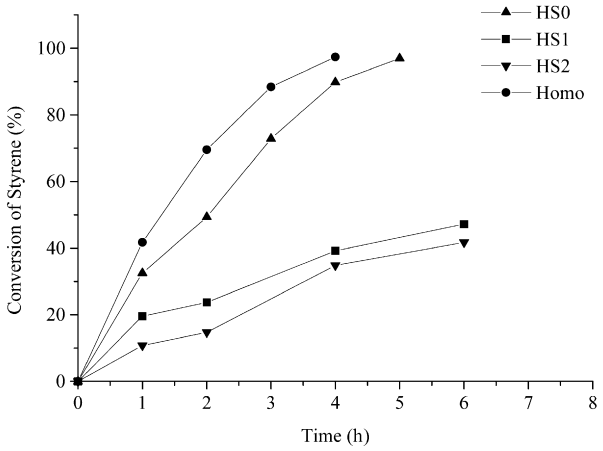

Fig. 8. Catalytic activity of HSn ($n = 0, 1, 2$) and $HRh(CO)(PPh_3)_3$ catalysts.

dendrimers growing outside the SBA-15 channels due to the limited surface areas and space outside SBA-15 mesopores [11].

3.2. Catalytic activity

HS0, HS1, HS2, and homogeneous $HRh(CO)(PPh_3)_3$ catalysts were applied for the hydroformylation of styrene at 60 °C under 20 bar of syn-gas (CO:H_2 ratio of 1:1). Fig. 8 shows the conversion of styrene as a function of reaction time for the four reactions. The HSn catalysts were run to study the difference of catalytic behavior between the passivated and nonpassivated dendritic SBA-15-supported rhodium catalysts. An equivalent amount of homogeneous $HRh(CO)(PPh_3)_3$ catalyst also was applied to compare the performance of the heterogeneous and homogeneous catalyst systems.

Fig. 8 shows that the HS0 catalyst was much more active than the HS1 and HS2 catalysts. Although the activity of HS0 was already close to that of $HRh(CO)(PPh_3)_3$, the greatest catalytic activity demonstrated by HS0 also corresponded to its greatest leaching of Rh species among the three heterogenized catalysts. According to the ICP results, 32.61% of the rhodium was lost from the fresh HS0 during the reaction, indicating that HS0's quasi-homogeneous catalytic activity is due mainly to the leaching of rhodium species to the liquid phase. This high leaching can be attributed mainly to the nonpassivated dendritic SBA-15 support, which tethered most of $HRh(CO)(PPh_3)_3$ outside the SBA-15 pores. This result is similar to previously reported findings on the tethering of $HRh(CO)(PPh_3)_3$ onto the nonpassivated MCM-41 support functionalized with surface amine ligands [6].

The catalytic activity of HSn catalysts decreased from HS0 to HS2 in a similar order as the leaching of rhodium species from the catalysts. This result indicates that the higher generation of PAMAM dendrimer grafted onto SBA-15 helped retain the grafted rhodium complexes better than those grafted on the lower generation of dendrimer. This finding also demonstrates that the homogeneous phase reaction dominated its heterogeneous counterpart

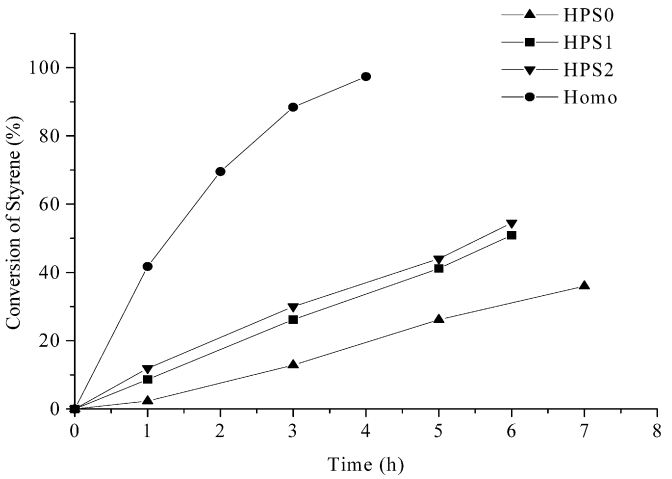

Fig. 9. Catalytic activity of HPSn ($n = 0, 1, 2$) and $HRh(CO)(PPh_3)_3$ catalysts.

in the hydroformylation reactions of styrene catalyzed by HSn catalysts.

Similarly, the HPSn catalysts also were used for the hydroformylation of styrene at the same reaction conditions as used for the HSn catalysts. The HPSn catalysts were evaluated to study the influence of pore size distribution and PAMAM generation on the hydroformylation reaction of styrene. Fig. 9 illustrates the conversion of styrene as a function of reaction time for the HPSn catalysts. In contrast to the order of the catalytic performance over HSn catalysts, which was the same as that of the amount of leaching, the order of catalytic activity of the HPSn catalysts was HPS2 > HPS1 > HPS0, exactly the opposite order than that of the amount of Rh leaching (i.e., HPS2 < HPS1 < HPS0). Although the HPS2 catalyst exhibited the least amount of leaching of rhodium species from the catalyst during the hydroformylation reaction, the HPS2 catalyst had the highest catalytic activity among the three HPSn catalysts. This finding demonstrates that the HPSn catalysts catalyze the hydroformylation reaction heterogeneously.

Based on the XPS results shown in Fig. 5, the BE values for the HPSn catalysts were very close, suggesting similar electronic properties of the catalytic species on these catalysts. The difference in the catalytic activity of these three HPSn catalysts, in which the catalytic activity increased with increasing dendrimer generation, may be attributed to the steric factor, due to the increasing length of the arms of grafted dendrimers inside the SBA-15 mesopores.

We also found that the heterogeneous HPSn catalysts exhibited lower catalytic activity than the homogeneous $HRh(CO)(PPh_3)_3$ catalyst. One possible reason for this is that the surface amine ligand $-NH_2$, which is more basic than PPh_3, coordinated with Rh species; the more basic $-NH_2$ would then make the Rh–CO bond stronger and CO dissociation more difficult, leading to decreased catalytic activity of the grafted rhodium complex on the surface-aminated SBA-15 support [30]. The other reason is that although HPSn catalysts have large surface areas and more multiple binding sites, which promote the dispersion of the rhodium complexes, the absolute amount of tethered rhodium species responsible for hydroformylation reaction was smaller in the HPSn catalysts than that in the homogeneous $HRh(CO)(PPh_3)_3$ catalytic system.

Furthermore, in contrast to the behavior of HSn catalysts, the catalytic activity of HPSn catalysts increased with increasing generations of grafted PAMAM dendrimer. In contrast, the appreciable increase in catalytic activity observed from the HPS0 to HPS1 catalysts due to the positive dendrimer effect differed from the decreased catalytic activity seen for the HS0 to HS1 catalysts due to the negative dendrimer effect. Although the HPS1 catalyst has a smaller pore size, less surface area, and less contribution from ho-

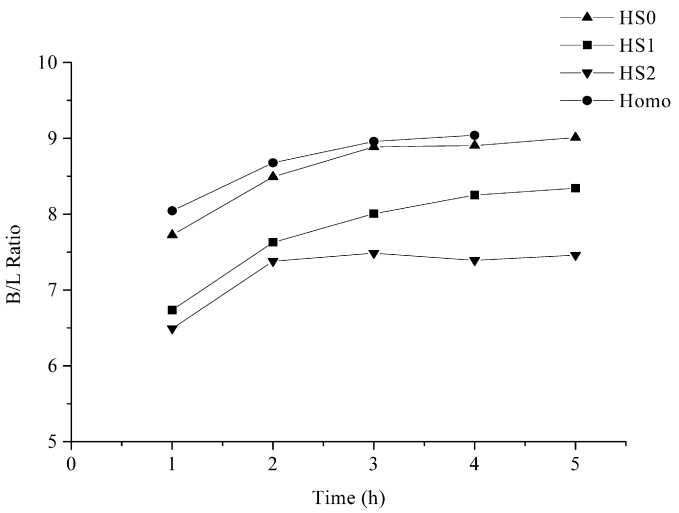

Fig. 10. Catalytic regio-selectivity of HS*n* ($n = 0, 1, 2$) and $HRh(CO)(PPh_3)_3$ catalysts. (Here B signifies branch aldehyde product 2-phenylpropionaldehyde and L signifies linear aldehyde product 3-phenylpropionaldehyde.)

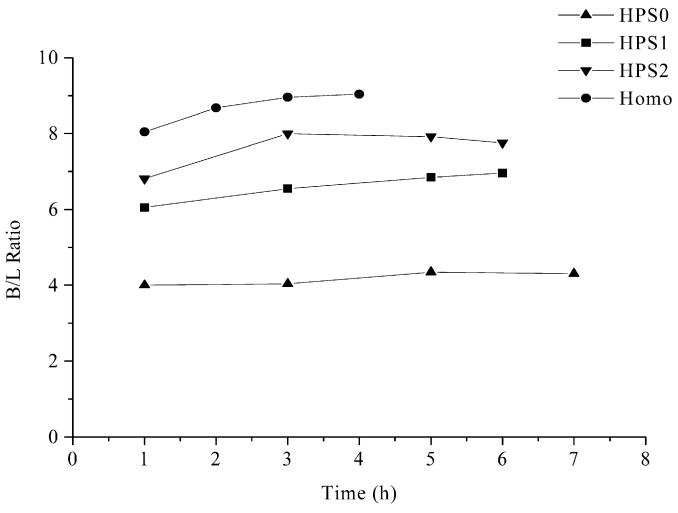

Fig. 11. Catalytic regio-selectivity of HPS*n* ($n = 0, 1, 2$) and $HRh(CO)(PPh_3)_3$ catalysts.

Table 4
ICP analysis of dendritic SBA-15 supported rhodium catalysts

Catalyst	Rh% (before reaction)	Rh% (after reaction)	Percent loss
HS0	1.726	1.163	32.61%
HS1	1.429	1.124	21.34%
HS2	1.388	1.129	18.66%
HPS0	1.127	0.972	13.75%
HPS1	1.367	1.234	9.73%
HPS2	1.249	1.230	1.52%
HPS2 (2nd cycle)	1.230	1.228	0.16%

mogeneous catalysis, the positive effect of internally grafted dendrimer helps accelerate the catalytic activity of HPS1 catalyst for styrene hydroformylation [31]. This is attributed to the perfect growth of PAMAM dendrimer inside the SBA-15 channels, which provides for better dispersion of rhodium complexes on the binding sites at the peripheries of the PAMAM dendrimers from the zeroth to the first generation. However, the slight increase in catalytic activity seen from HPS1 to HPS2 indicates that this positive promotional effect reached the limit, likely due to the bulkiness of the second-generation dendrimer inside the microenvironment of the SBA-15 channels [14].

3.3. Catalytic selectivity

Fig. 10 shows the following regioselectivity order of the HS*n* catalysts: HS0 > HS1 > HS2. This is the same order as the order of catalytic activity. This order of regioselectivity is also reminiscent of the $RhCl(PPh_3)_3$ catalysts supported on dendritic SBA-15 supports [13]. Based on the ICP results (Table 4), the highest regioselectivity exhibited by the HS0 catalyst can be attributed to the high amount of rhodium species that leached into the liquid phase from the nonpassivated dendritic SBA-15 support. As the generation of grafted PAMAM dendrimer increased, the amount of rhodium species leaching to the solution decreased due to the increased retention power of longer dendrimer arms. Accordingly, the regioselectivity of the HS1 and HS2 catalysts decreased with increasing generations of grafted PAMAM dendrimer on the nonpassivated SBA-15. All of these results indicate that homogeneous hydroformylation, which was dominant in the HS*n* catalyst system, was mainly responsible for the high regioselectivity of the HS*n* catalysts.

The support properties also were found to influence regioselectivity. Our BET results revealed smaller surface areas for the HS*n* catalysts compared with the HPS*n* catalysts. The HS*n* catalysts exhibited severe cross-linking of dendrimers outside the pores, leading to a congested microenvironment that is sterically negative for regioselectivity. Therefore, an increase in local steric congestion occurred from HS0 to HS2, due to shrinking surface areas and increasing dendrimer volume.

Fig. 10 also shows that within the first 3 h of reaction, all HS*n* catalysts exhibited an appreciable increase in regioselectivity, indicating intensified leaching of rhodium species to the liquid phase of the reaction under the reaction conditions. In contrast, Fig. 11 shows that the regioselectivity of HPS*n* catalysts remained quite constant over time, suggesting that the HPS*n* catalyst was more stable and exhibited much less leaching of rhodium species into the liquid phase, as was confirmed by the ICP test.

It is noteworthy that, according to Fig. 11, the regioselectivity of the HPS*n* catalysts increased from a zeroth-generation to a second-generation internally grafted dendrimer. This order was the same as their order of activity: HPS0 < HPS1 < HPS2. Although the three passivated HPS*n* catalysts were less selective than the homogeneous precursor $HRh(CO)(PPh_3)_3$, the HPS2 catalyst demonstrated very high regioselectivity, close to that of $HRh(CO)(PPh_3)_3$. Because the ICP results indicate much less leaching of rhodium species from the HPS2 catalyst, the catalyst's high regioselectivity can be attributed to the influence of the second-generation internally grafted dendrimer, which may provide better flexibility of dendrimer arm and better dispersion of tethered rhodium species.

But the promotional effect due to the dendritic support cannot be increased by increasing dendrimer generation without limits, due to the limited pore size and volume of the SBA-15 mesopores [10]. Of the three passivated HPS*n* catalysts, the HPS2 catalyst proved to be the most selective, active, and stable heterogenized rhodium catalyst. Because this catalyst has the smallest pore size distribution, future investigation into the effect of pore size on the catalytic performance would be worthwhile.

3.4. Characterization of used catalysts

Fig. 12 shows that the Rh $3d_{5/2}$ BEs of all used catalysts applied to the hydroformylation of styrene shifted to lower values centered at 307.55 eV (±0.1 eV). These values are very close to those for Rh^{+1} complexes. Knozinger proposed a $L_nRh^{+1}(CO)_2$ general form for the silica-supported rhodium complexes with Rh $3d_{5/2}$ binding energies ranging from 307.0 to 307.6 eV [32]. Therefore,

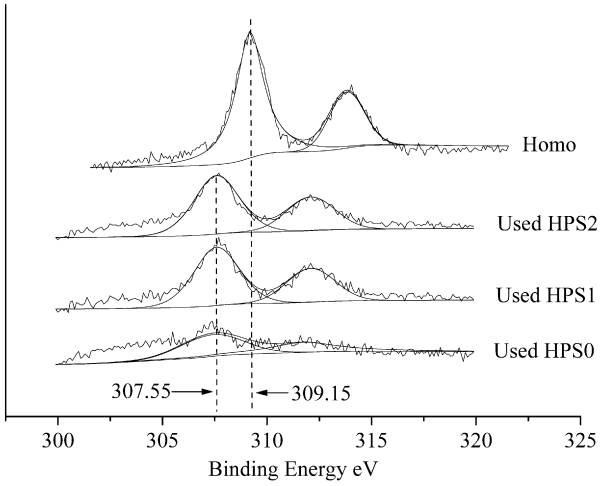

Fig. 12. XPS spectra of used HPS*n* catalysts ($HRh(CO)(PPh_3)_3$ as reference).

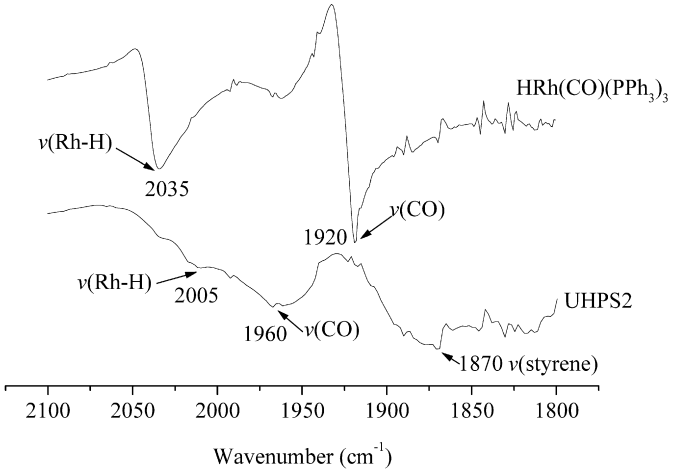

Fig. 13. FTIR spectra of $HRh(CO)(PPh_3)_3$ and used HPS2 (UHPS2).

the supported rhodium complexes observed in this study may be transformed into a similar $L_nRh^{+1}(CO)_x$ form during the styrene hydroformylation reaction. Amine ligands can replace one or two phosphine ligands coordinated to the Rh during the transformation, because the surface amine ligand of dendrimer is a stronger σ-electron donor than the phosphine ligand. Because phosphine ligand is a stronger π acid than amine ligand, the d–π backdonation is decreased with the replacement of PPh_3 by $-NH_2$, and thus the BEs of Rh $3d_{5/2}$ shift to lower values.

Because the used HPS*n* catalysts exhibited characteristic rhodium spectra with appreciable intensity, the change in the BEs of Rh $3d_{5/2}$ indicates that a considerable amount of rhodium species was retained in the passivated dendritic SBA-15 supports.

Fig. 13 shows the FTIR spectra of used HPS2 with $HRh(CO)(PPh_3)_3$ as the reference. The used HPS2 catalyst exhibited a peak at 1960 cm^{-1}, which is assigned to terminal υ(CO). This peak showed a decrease of 15 cm^{-1} from the υ(CO) of the fresh HPS2 (Fig. 6), indicating that the Rh center of the used catalyst was more electron-rich. This FTIR finding is consistent with the XPS results for the used HPS*n* catalysts. The used HPS2 catalyst also exhibited a shoulder peak at around 2005 cm^{-1}, which may be assigned to the υ(Rh–H), given that it was of similar frequency to the Rh–H peak of the fresh HPS2. This finding indicates that the rhodium hydride species was the predominant intermediate species of the catalytic cycle. The broad peak at around 1870 cm^{-1} is assigned to the unreacted styrene on the used catalyst.

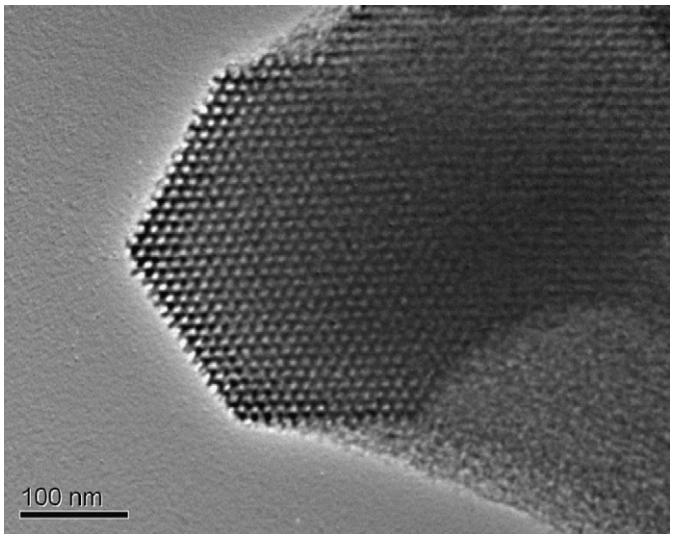

Fig. 14. TEM image of used HPS2 catalyst.

Table 4 gives the ICP analysis results of the percentage of Rh in the HS*n* and HPS*n* catalysts before and after the hydroformylation of styrene. These results show much less leaching of rhodium in the HPS*n* catalysts than in the HS*n* catalysts. The relatively high leaching of rhodium from the nonpassivated dendritic SBA-15 supports can be attributed to the tethering of $HRh(CO)(PPh_3)_3$ at the dendrimers' peripheries outside the SBA-15 pore channels, because the externally tethered rhodium complex species could readily leach without pore confinement. But because the binding sites of the HPS0, HPS1, and HPS2 catalysts are available only inside the SBA-15 channels, the rhodium complexes are tethered inside the pore channels, resulting in encapsulated rhodium complexes that are well protected from leaching into the liquid phase by the mesopore walls. These findings are in agreement with those for the SBA-15-supported $RhCl(PPh_3)_3$ catalysts [13].

We chose the most active and selective HPS2 catalyst for the molecular stability test of the encapsulated rhodium complex catalyst after two recyclings of the hydroformylation reaction. The ICP results for the used HPS2 catalyst show that the loss of Rh from HPS2 catalyst not only was minimal, but also decreased from slightly above 1 wt% (i.e., 1.52 wt%) for the first cycle to almost negligible (i.e., 0.16 wt%) for the second cycle. This result demonstrates that the $HRh(CO)(PPh_3)_3$ catalyst tethered inside the mesopores of dendritic SBA-15 was robust during the hydroformylation reaction, indicating that the second-generation dendrimer grown inside the mesopores of HPS2 was of optimal length and crowdedness to retain the rhodium complex inside the dendritic mesopores of SBA-15.

In Fig. 14, the TEM image of the used HPS2 catalyst also confirms the stability of the mesoporous structure of the SBA-15 support during the styrene hydroformylation reaction. The stability of the SBA-15 mesopores helps protect the encapsulated rhodium complexes tethered on the internally grafted dendrimer from leaching into the liquid-phase solution during the course of the hydroformylation reaction.

4. Conclusion

The passivation of silanols outside the SBA-15 channels resulted in a dendritic support tethering most of the rhodium complex inside the mesopores, leading to the HPS*n* catalysts, which catalyze the hydroformylation reaction only inside the SBA-15 channels, with much less leaching of rhodium species. In contrast, the nonpassivated dendritic SBA-15 catalysts HS*n*, in which the silanols

outside the pore channels have not been passivated, demonstrated the significant drawback of leaching of rhodium species into the liquid phase. The higher activity and selectivity of the HS*n* catalysts compared with the HPS*n* catalysts can be attributed to the greater leaching of rhodium from the HS*n* catalysts. A positive dendrimer effect also was observed for the HPS*n* catalysts, with the following order of activity: HPS2 > HPS1 > HPS0. All of these results suggest that dendrimers grown inside the mesoporous channels help increase the catalytic activity, selectivity, and stability of the heterogenized rhodium catalysts for hydroformylation reactions.

References

[1] P. Eilbracht, L. Barfacker, C. Buss, C. Hollmann, B.E. Kitsos-Rzychon, C.L. Kranemann, T. Rische, R. Roggenbuck, A. Schmidt, Chem. Rev. 99 (1999) 3329.
[2] D. Evans, G. Yagupsky, G. Wilkinson, J. Chem. Soc. A 12 (1968) 2660.
[3] S.C. Bourque, F. Maltais, W. Xiao, O. Tardif, H. Alper, P. Arya, L.E. Manzer, J. Am. Chem. Soc. 121 (1999) 3035.
[4] H.C. Foley, S.J. Decanio, K.D. Tau, K.J. Chao, J.H. Onuferko, C. Dybowski, B.C. Gates, J. Am. Chem. Soc. 105 (1983) 3074.
[5] S.M. Lu, H. Alper, J. Am. Chem. Soc. 125 (2003) 13126.
[6] K. Mukhopadhyay, A.B. Mandale, R.V. Chaudhari, Chem. Mater. 15 (2003) 1766.
[7] J.P.K. Reynhardt, Y. Yang, A. Sayari, H. Alper, Chem. Mater. 16 (2004) 4095.
[8] N. Brinkmann, D. Giebel, G. Lohmer, M.T. Reetz, U. Kragl, J. Catal. 183 (1999) 163.
[9] H. Sellner, K. Hametner, D. Gunther, D. Seebach, J. Catal. 215 (2003) 87.
[10] D.Y. Zhao, Q. Huo, J.L. Feng, B.F. Chmelka, G.D. Stucky, J. Am. Chem. Soc. 120 (1998) 6024.
[11] D.S. Shephard, W.Z. Zhou, T. Maschmeyer, J.M. Matters, C.L. Roper, S. Parsons, B.F.G. Johnson, M.J. Duer, Angew. Chem. Int. Ed. Engl. 37 (1998) 2719.
[12] T. Maschmeyer, R.D. Oldroyd, G. Sankar, J.M. Thomas, I.J. Shannon, J.A. Klepetko, A.F. Masters, J.K. Beattie, C.R.A. Catlow, Angew. Chem. Int. Ed. Engl. 36 (1997) 1639.
[13] P. Li, S. Kawi, Catal. Today 131 (2008) 61.
[14] Y.C. Xiao, T.S. Chung, M.L. Chng, Langmuir 20 (2004) 8230.
[15] L. Huang, S. Kawi, Catal. Lett. 90 (2003) 165.
[16] V. Antochshuk, M. Jaroniec, Chem. Commun. (1999) 2373.
[17] R. Schmidt, E.W. Hansen, M. Stocker, D. Akporiaye, O.H. Ellestad, J. Am. Chem. Soc. 117 (1995) 4049.
[18] C.P. Jaroniec, M. Kruk, M. Jaroniec, A. Sayari, J. Phys. Chem. B 102 (1998) 5503.
[19] K. Mukhopadhyay, R.V. Chaudhari, J. Catal. 213 (2003) 73.
[20] M.J. Burk, A. Gerlach, D. Semmerji, J. Org. Chem. 65 (2000) 8933.
[21] Y.S. Varshavsky, T.G. Cherkasova, I.S. Podkorytov, Inorg. Chem. Commun. 7 (2004) 489.
[22] K.A. Chatziapostolou, K.A. Vallianatou, A. Grigoropoulo, C.P. Raptopoulou, A. Terzis, I.D. Kostas, P. Kyritsis, G. Pneumatikakis, J. Organomet. Chem. 692 (2007) 4129.
[23] S.K. Sharma, V.K. Srivastava, R.S. Shukla, P.A. Parikh, R.V. Jasra, New J. Chem. 31 (2007) 277.
[24] P.J. Scott, G.L. Rempel, Macromolecules 25 (1992) 2811.
[25] I.T. Horvath, R.V. Kastrup, A.A. Oswald, Catal. Lett. 2 (1989) 85.
[26] A.M. Trzeciak, Z. Olejnik, J.J. Ziókowski, T. Lis, Inorg. Chim. Acta 350 (2003) 339.
[27] S.S. Bath, L. Vasaka, J. Am. Chem. Soc. 65 (1963) 3500.
[28] L. Damonese, M. Datt, M. Green, C. Steenkamp, Coordin. Chem. Rev. 248 (2004) 2393.
[29] J.P.K. Reynhardt, H. Alper, J. Org. Chem. 68 (2003) 8353.
[30] A.C. Da Silva, K.C.B. de Oliveira, E.V. Gusevskaya, E.N. dos Santos, J. Mol. Catal. A: Chem. 179 (2002) 133.
[31] R. Breinbauer, E.N. Jacobsen, Angew. Chem. Int. Ed. Engl. 39 (2000) 3604.
[32] H. Knozinger, Inorg. Chim. Acta 37 (1979) 537.